

Evaluation of Split-Window Land Surface Temperature Algorithms for Generating Climate Data Records

Yunyue Yu, Jeffrey L. Privette, *Member, IEEE*, and Ana C. Pinheiro

Abstract—Land surface temperature (LST) is a key indicator of the Earth's surface energy and is used in a range of hydrological, meteorological, and climatological applications. As needed for most modeling and climate analysis applications, LST products that are generated from polar-orbiting meteorological satellite sensors have spatial resolutions from several hundred meters to several kilometers and have (quasi) daily temporal resolution. These sensors include the National Oceanic and Atmospheric Administration Advanced Very High Resolution Radiometer (AVHRR), the Earth Observing System Moderate Resolution Imaging Spectroradiometer (MODIS), and the forthcoming Visible/Infrared Imager Radiometer Suite (VIIRS) series, to be flown onboard the National Polar-Orbiting Operational Environmental Satellite System (VIIRS flights begin approximately 2009). Generally, split-window algorithms are used with these sensors to produce LST products. In this paper, we evaluated nine published LST algorithms (or, in some cases, their slight variants) to determine those that are most suitable for generating a consistent LST climate data record across these satellite sensors and platforms. A consistent set of moderate-resolution atmospheric transmission simulations were used in determining the appropriate coefficients for each algorithm and sensor (AVHRR, MODIS, and VIIRS) combination. Algorithm accuracy was evaluated over different view zenith angles, surface-atmosphere temperature combinations, and emissivity errors. Both simulated and actual remote sensing data were used in the evaluation. We found that the nine heritage algorithms can effectively be collapsed into three groups of highly similar performance. We also demonstrated the efficacy of an atmospheric path-length correction term that is added to the heritage algorithms. We conclude that the algorithms depending on both the mean and difference of band emissivities (Group 1 in our nomenclature) are most accurate and stable over a wide range of conditions, provided that the emissivity can be well estimated *a priori*. Where the emissivity cannot be well estimated, the Group 3 algorithms (which do not depend on the emissivity difference) modified with the path-length correction term perform better.

Index Terms—Climate data record (CDR), land surface temperature (LST), radiative transfer simulation model, split-window (SW) algorithm.

I. INTRODUCTION

LAND surface temperature (LST) products are routinely generated from moderate-resolution satellite data (e.g., Moderate Resolution Imaging Spectroradiometer (MODIS) on the National Aeronautics and Space Administration's (NASA) Terra and Aqua platforms, Advanced Along-Track Scanning Radiometer on the European Space Agency's Environmental Satellite) because they indicate the surface energy that is available at the land-atmosphere interface [1]. This information can be used to help assess surface-atmosphere fluxes (e.g., water, carbon) [2], root-zone soil moisture, and to reveal climatological trends when considered in a multiyear time series [2]. The latter application is among the most demanding because climatological changes tend to be small and can often be obscured by noise and natural LST variability.

To meet the data demands of climate-change monitoring and science, the science community has increasingly called for unified global products generated from a sequence of satellites using "best practice" algorithms [4], [5]. Such products are termed climate data records (CDRs) and can be more formally defined as a "time series of measurements of sufficient length, consistency, and continuity to determine climate variability and change" [4]. NASA uses the same concept to define its Earth System Data Records (<http://lcluc.umd.edu/products/Land%5FESDR/>).

Several satellite CDRs already exist [5]. For example, Stolarski and Frith [6] produced an ozone CDR extending from 1978 to 2006 through rigorous intercalibration of data from solar backscatter ultraviolet and total ozone mapping spectrometers. Casey and Reynolds [7] developed a relatively seamless 20-year CDR of sea surface temperature (SST) by reprocessing the complete National Oceanic and Atmospheric Administration (NOAA) data archive as algorithm accuracy and sensor calibration knowledge improved. These products can be readily used for climate analysis and model forcing or assessment.

The development of a long-term moderate-resolution LST record is likely best accomplished by using a succession of polar-orbiting satellite sensors, including the Advanced Very High Resolution Radiometer (AVHRR) (1978 to present), MODIS (2000 to present), and extending forward with Visible/Infrared Imager Radiometer Suite (VIIRS) (expected

Manuscript received October 20, 2006; revised July 24, 2007. This work was supported by the National Aeronautics and Space Administration National Polar-Orbiting Operational Environmental Satellite System Preparatory Project Science Team and the National Oceanic and Atmospheric Administration Geostationary Operational Environmental Satellite Series R Algorithms Working Group.

Y. Yu is with the National Environmental Satellite, Data, and Information Service Center for Satellite Applications and Research, National Oceanic and Atmospheric Administration, Camp Springs, MD 20746 USA (e-mail: yunyue.yu@noaa.gov).

J. L. Privette and A. C. Pinheiro are with the National Environmental Satellite, Data, and Information Service National Climate Data Center, National Oceanic and Atmospheric Administration, Asheville, NC 28801-5001 USA (e-mail: jeff.privette@noaa.gov; Ana.Pinheiro@noaa.gov).

Digital Object Identifier 10.1109/TGRS.2007.909097

service from 2010 to approximately 2026). These sensors are manifested on NOAA's Polar-Orbiting Environmental Satellites (POESs), NASA's Earth Observing System (EOS) Terra and Aqua satellites, and the future National POES System (NPOESS) satellites, respectively. The first VIIRS launch will be on the NPOESS Preparatory Project (NPP) (launch planned for 2009), a four-instrument pathfinder version of an NPOESS platform. Although NOAA plans just one more AVHRR launch, the European Organisation for the Exploitation of Meteorological Satellites will continue AVHRR observations on its three successive meteorological operational satellite platforms, with the first one scheduled to begin on-orbit operations in spring 2007. Together, the three basic sensor designs will provide a 50-year continuous data record (assuming full-NPOESS implementation).

To estimate the surface "skin" temperature from these sensors, most scientists rely on "split-window" (SW) algorithms that are derived from a first-order Taylor-series linearization of the radiative transfer equation in long-wave infrared spectral bands [8]. The SW algorithms effectively provide atmospheric correction of a brightness temperature measurement in one spectral band (typically centered around $11\text{-}\mu\text{m}$) given a brightness temperature measurement in a second "spectrally close" band (typically centered around $12\text{-}\mu\text{m}$). They exploit the tendency of atmospheric absorption to change more rapidly in spectral space than in surface emissivity. The SW technique is particularly favored for its simplicity and robustness. In most cases, the SW LST algorithms simultaneously convert brightness temperatures to skin temperatures, given the estimates of the surface spectral emissivity.

Many flavors of the SW algorithms have been developed in the past 15 years, and together, they provide a starting point for developing a reliable and accurate CDR algorithm. Several studies have intercompared published algorithms. For example, Ouaidrari *et al.* [9] compared LST algorithms in their AVHRR LST Pathfinder II data set and found that some SW LST equations were less accurate for atmospheres with high water vapor content. Vazquez *et al.* [10] showed that errors in surface emissivities propagate through each algorithm in different manners. Kerr [11] also performed an algorithm comparison and concluded that selecting the best LST algorithm may depend on knowledge of uncertainties in the water vapor and the surface emissivity.

Unfortunately, each of the studies focused only on AVHRR and was limited in a climatic and geographic scope. Although a CDR algorithm that is applicable to multiple sensors (AVHRR, MODIS, and VIIRS) should indeed leverage past advancements, much work remains. Specifically, it is not clear which of the published algorithms is the most accurate and robust across the different sensors, given their unique characteristics (e.g., bandpass widths and centers). New CDR-focused studies must consider the full range of the Earth's land and atmosphere combinations. Furthermore, CDR products must be decontaminated from sensor and orbit artifacts. For example, LST angular anisotropy was recently found in daily AVHRR products over continental Africa [12]. These effects will vary for each sensor type because each has a unique orbit and sampling geometry. Finally, the conversion from brightness temperature to kinetic

temperature, which is intrinsic to an LST algorithm, requires knowledge of the surface spectral emissivity. This parameter is very difficult to measure at scales commensurate with moderate-resolution satellite sensors. To our knowledge, all the operational emissivity maps that are used with these sensors are based on laboratory measurements. New approaches for the dynamic estimation of emissivity from MODIS [13] are not yet proven. Either way, it is likely that significant errors are present in current maps. The sensitivity of the retrieved LST to these errors varies with the algorithm and sensing system.

In this paper, we addressed several of the aforementioned issues. Specifically, we sought to identify the most suitable SW algorithm for simultaneous use with AVHRR, MODIS, and VIIRS. Therefore, we systematically evaluated and compared nine published algorithms (or their slight variants) developed for moderate-resolution sensors. We created nine additional algorithms by adding an atmospheric path-length correction term to each published algorithm. The resulting 18 algorithms were intercompared using simulated data, actual MODIS observations and products, and the algorithms' mathematical differentials with respect to surface emissivity (the input parameter with the greatest uncertainty).

We evaluated and compared the algorithms' performance as a function of:

- 1) the spectral response functions of AVHRR (NOAA-14, -16), MODIS (Aqua and Terra), and VIIRS (predicted);
- 2) cold (drier) versus warm (moister) atmospheric states;
- 3) view zenith angle;
- 4) $T_s - T_{\text{air}}$, i.e., the difference between LST and surface air temperature (SAT) (2 m above ground level);
- 5) surface emissivity errors.

Following a description of the sensors, algorithms, path-length correction term, and simulated satellite data, we compare the algorithms according to the aforementioned criteria. We then describe the performance results. We discuss these results vis-à-vis the algorithm functional forms. Based on a comprehensive simulation analysis and MODIS data evaluation, we recommend algorithms that are well suited for CDR development and discuss considerations for adapting one algorithm for use with the different sensors. Finally, we conclude with our recommendation of the algorithm for CDR use.

II. ALGORITHMS AND DATA

A. AVHRR, MODIS, VIIRS Sensors

The sensors considered in this paper share some general characteristics, but have different designs and band specifications. Each is a "whisk-broom"-type scanner ($\pm\sim 56^\circ$) with moderate-resolution sampling (see Table I) and ground swaths of 3399, 2330, and 3040 km (AVHRR, MODIS, and VIIRS, respectively). The operational AVHRR sensor, which was originally designed in 1978 and updated twice since, has one detector per spectral band. This design requires a relatively fast scan rate and, hence, a relatively wide spectral bandpass (Table I). MODIS, which was designed as a state-of-the-art research sensor in the 1990s, has ten along-track detectors per thermal spectral band. Its scan rate is slower, and its bandpasses are narrower

TABLE I
SPECTRAL AND SPATIAL RESOLUTIONS OF AVHRR, MODIS,
AND VIIRS THERMAL INFRARED BANDS

AVHRR-3			MODIS			VIIRS		
Band	Spectral Bandpass* (μm)	HSR#	Band	Spectral Bandpass (μm)	HSR	Band	Spectral Bandpass (μm)	HSR (m)
4	10.300 - 11.300	1100	31	10.780 - 11.280	1000	M15	10.263 - 11.263	750
5	11.500 - 12.500	1100	32	11.770 - 12.270	1000	M16	11.538 - 12.488	750

* Full Width Half Maximum positions

HSR=Horizontal Spatial Resolution at nadir, commonly referred to as pixel size (per side)

TABLE II
PUBLISHED LST ALGORITHMS EVALUATED IN THIS PAPER. ADOPTED ALGORITHMS (EXACTLY THE SAME EXCEPT THE CONSTANT TERM): 1, 3, 5, 11, 15, 17. ADAPTED ALGORITHMS (WITH SLIGHT MODIFICATIONS): 7, 9, 13

No	Formula#	Reference of Algorithm Adaption
1	$T_s = C + (A_1 + A_2 \frac{1 - \epsilon}{\epsilon} + A_3 \frac{\Delta \epsilon}{\epsilon^2})(T_{11} + T_{12}) + (B_1 + B_2 \frac{1 - \epsilon}{\epsilon} + B_3 \frac{\Delta \epsilon}{\epsilon^2})(T_{11} - T_{12})$	Wan <i>et al.</i> [14]; Becker & Li [15]
3	$T_s = C + A_1 \frac{T_{11}}{\epsilon} + A_2 \frac{T_{12}}{\epsilon} + A_3 \frac{1 - \epsilon}{\epsilon}$	Prata & Platt [16]; modified by Caselles <i>et al.</i> [17]
5	$T_s = C + A_1 T_{11} + A_2 (T_{11} - T_{12}) + A_3 (1 - \epsilon) + A_4 \Delta \epsilon$	Ulivieri <i>et al.</i> [18]
7	$T_s = C + A_1 T_{11} + A_2 (T_{11} - T_{12}) + A_3 \frac{1 - \epsilon}{\epsilon} + A_4 \frac{\Delta \epsilon}{\epsilon^2}$	Vidal [19]
9	$T_s = C + A_1 T_{11} + A_2 (T_{11} - T_{12}) + A_3 (T_{11} - T_{12})(1 - \epsilon_{11}) + A_4 T_{12} \Delta \epsilon$	Price [20]
11	$T_s = C + A_1 T_{11} + A_2 (T_{11} - T_{12}) + A_3 \epsilon$	Uliveri <i>et al.</i> [21]
13	$T_s = C + A_1 T_{11} + A_2 (T_{11} - T_{12}) + A_3 \epsilon + A_4 \frac{\Delta \epsilon}{\epsilon}$	Sobrino <i>et al.</i> [22]
15	$T_s = C + A_1 T_{11} + A_2 (T_{11} - T_{12}) + A_3 (1 - \epsilon_{11}) + A_4 \Delta \epsilon$	Coll <i>et al.</i> [23]
17	$T_s = C + A_1 T_{11} + A_2 (T_{11} - T_{12}) + A_3 (T_{11} - T_{12})(T_{11} - T_{12}) + A_4 (1 - \epsilon_{11}) + A_5 \Delta \epsilon$	Sobrino <i>et al.</i> [24]

T_s is the retrieved LST; T_{11} and T_{12} are the brightness temperatures at bands 11 μm and 12 μm, respectively; $\epsilon = (\epsilon_{11} + \epsilon_{12})/2$, $\delta \epsilon = \epsilon_{11} - \epsilon_{12}$; ϵ_{11} and ϵ_{12} are emissivity values at bands 11 μm and 12 μm, respectively; A , B , and C 's are regression coefficients.

(Table I). This potentially allows more accurate correction of atmospheric effects relative to AVHRR. VIIRS, like AVHRR, is designed for operational use and has similar bandpasses. It has 16 along-track detectors per thermal spectral band (Table I). The sensors' horizontal spatial resolutions, or the ground instantaneous fields of view, are also provided in Table I.

The sensors have other differences in their thermal bands, including the dynamic ranges, signal-to-noise ratios, quantization, precision, geolocation and band-to-band registration. These characteristics, however, are peripheral to the current paper.

B. SW LST Algorithms

We considered many SW LST algorithms from the published literature [14]–[24] and adapted nine for our analysis

(see Table II). The adapted algorithms, which are noted in the table, were slightly modified from the originals for having better separation within the nine algorithms. These algorithms are hereafter referred to as the “base algorithms.” The heritage algorithms for these were typically developed with different assumptions and approximations and tested under different environmental conditions. As the theoretical underpinnings are not germane to our study, we refer readers to the original publications for their development details.

The published coefficients of these algorithms were typically determined by regression using simulated top-of-atmosphere (TOA) brightness temperatures, together with the prescribed model LST values. The coefficients were developed for use with just one sensor. Because our paper concerns the applicability over multiple sensors, we chose to reregress the algorithms using a common database (described hereafter). This approach

also eliminates biases from inconsistent regression approaches or databases among the algorithm developers.

C. Correcting for Path Angle Variability

As previously noted, the sensors considered here have wide fields of view. McClain *et al.* [25] first pointed out that, at high viewing angles, atmospheric absorption may be amplified. Geometric analysis shows that the atmospheric path length at the sensor's edge-of-scan is at least 2.5 times higher than at nadir. Path water vapor generally increases approximately proportionally. If an SW algorithm's coefficients are determined for typical water vapor amounts in the vertical column, then algorithm accuracy can significantly degrade at large view angles. Of the base algorithms, only the standard MODIS algorithm addresses this problem [14]. Specifically, the MODIS algorithm uses unique equation coefficients determined for each 10° view angle subrange (e.g., 0° – 10° , 10° – 20° , etc.).

An alternative way to address the magnification of water vapor effects with increasing view angle is to add a path-length correction term to the SW formulation. For SST retrieval, Walton *et al.* [26] pointed out that, whereas the multiplicative factor $(T_{11} - T_{12})$ has been empirically found to improve the accuracy of the SW equation, a term with the satellite zenith angle provides an empirical correction for the off-nadir path-length amplification effect. Recently, developers of the NPOESS VIIRS LST SW algorithm applied a view zenith angle term as a path-length correction [27]. Sun and Pinker [28] proposed two SW LST algorithms for Geostationary Operational Environmental Satellite (GOES) satellites, which use a similar path-length correction term. Sun and Pinker also applied the algorithms to AVHRR data for temperature diurnal cycle studies [29]. Currently, the GOES-R Algorithm Working Group is using the path-length correction term in its LST algorithm development [30].

In the present paper, we used the path-length correction term of $(T_{11} - T_{12})(\sec \theta - 1)$, where $(T_{11} - T_{12})$ is the difference in TOA brightness temperatures in bands 11- and $12\text{-}\mu\text{m}$ (a quantity roughly proportional to the column atmospheric absorption), $(\sec \theta - 1)$ represents the path difference from nadir, and θ is the view zenith angle. We added the path-length term to each of the base algorithms, resulting in nine additional algorithms. We hereafter use even numbers (2, 4, ...) to identify the modified algorithms, where an even-numbered algorithm corresponds to the prior odd-numbered base algorithm with the added path-angle term. For instance, algorithm 8 corresponds to the base algorithm 7 with the added path-length term, i.e.,

$$T_s = C + A_1 T_{11} + A_2 (T_{11} - T_{12}) + A_3 \frac{1 - \varepsilon}{\varepsilon} + A_4 \frac{\Delta \varepsilon}{\varepsilon^2} + B (T_{11} - T_{12}) (\sec \theta - 1). \quad (1)$$

D. Satellite Data Simulation

To evaluate the algorithms in a consistent manner, we determined new coefficients for each algorithm from a com-

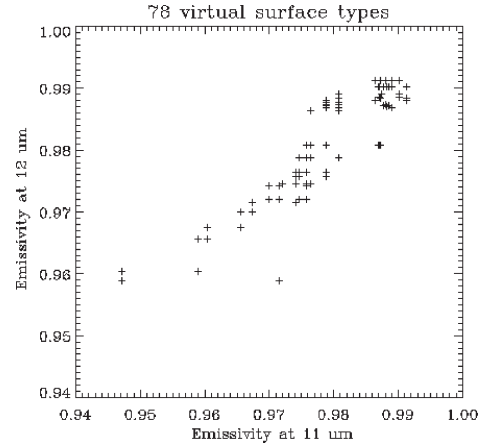


Fig. 1. Emissivity values of 78 virtual surface types. The values are generated by recombining the $\sim 11\text{-}$ and $\sim 12\text{-}\mu\text{m}$ spectral emissivity values from Snyder *et al.*'s [32] surface-type measurements.

mon set of model-generated data. We used the atmospheric radiative transfer model MODerate-resolution atmospheric TRANsmision (MODTRAN) (version 4, revision 1) [31] to determine the TOA radiances.

We defined 78 different land surface types by prescribing unique surface emissivity values. First, 26 spectral emissivity values at around 11- and $12\text{-}\mu\text{m}$ were calculated from Snyder *et al.*'s [32] emissivity classification data using the MODIS Aqua sensor response functions (bands 31 and 32). Of these, 14 represent the means of Snyder's 14 surface classes and the other 12 are those values combined with the estimated uncertainties [32] (two of them are not unique). In an effort to represent a wider range of the Earth's natural variability, we then recombined the 11- and $12\text{-}\mu\text{m}$ emissivity values from the different samples to construct additional 52 "virtual surface types." Each virtual surface type was manually determined through careful analysis of the variability in Snyder's original samples such that the virtual types were both realistic and yet had adequate variation. Fig. 1 shows the distribution of these emissivity values.

To prescribe atmospheric conditions, we used 60 daytime cloud-free radiosonde profiles from the CrIS F98-Weather Products Test Bed Data Package (NOAA88, Rev. 1.0, M. Goldberg, personal communication, 1998). The profiles represent a variety of atmospheric conditions, covering a column water vapor range of $0.5\text{--}5.8\text{ g/cm}^2$ and a SAT range of $260\text{--}304\text{ K}$. They were collected near 1000h and 1500h local time, which is close to the equator crossing times of the polar-orbiting satellites that are considered here. The selected profiles spanned a latitude range of $60^\circ\text{S--}70^\circ\text{N}$. For each atmospheric profile, we varied the prescribed LST as $T_{\text{air}} - 15\text{ K} < \text{LST} < T_{\text{air}} + 15\text{ K}$, where T_{air} is the SAT that is provided with the profiles. The range was chosen from Wan *et al.*'s [14] work and our own measurements in the field (primarily in Africa). For each $\Delta\text{LST} = 1\text{ K}$ increment in this range, we iterated the sensor view zenith angle from 0° to 70° , with a 10° increment.

TOA radiance values were calculated from each model run. The TOA spectral radiance $I(\lambda)$ was converted into a satellite sensor-received radiance $B(T, \lambda)$ by convolution with the

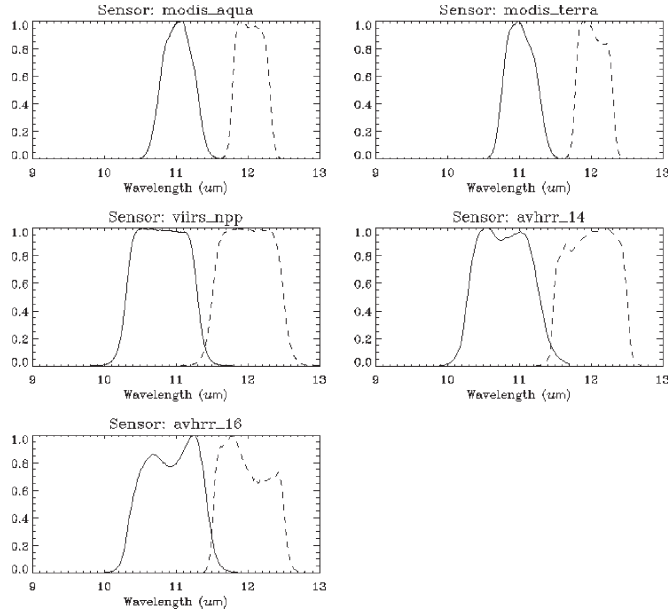


Fig. 2. Sensor relative spectral response functions of the thermal infrared bands for MODIS Aqua, MODIS Terra, VIIRS, AVHRR-14, and AVHRR-16.

sensor's relative spectral response function $RSR(\lambda)$. We applied the following formula for the conversion:

$$\bar{I}(T, \lambda_0) = \frac{\int_{\lambda_1}^{\lambda_2} I(\lambda) RSR(\lambda) d\lambda}{\int_{\lambda_1}^{\lambda_2} RSR(\lambda) d\lambda} \quad (2)$$

where λ_1 and λ_2 are the lower and upper limits of $RSR(\lambda)$, as shown in Fig. 2 for MODIS Aqua, MODIS Terra, VIIRS, AVHRR-14, and AVHRR-16. λ_0 is the central wavelength of the band defined as

$$\lambda_0 = \frac{\int_{\lambda_1}^{\lambda_2} \lambda \cdot RSR(\lambda) d\lambda}{\int_{\lambda_1}^{\lambda_2} RSR(\lambda) d\lambda} \quad (3)$$

The satellite brightness temperature for the band that is centered at wavelength λ_0 is calculated using the inversion of the Planck function definition

$$T = \left(\frac{hc}{k\lambda_0} \right) \frac{1}{\ln \left(\frac{2hc^2\lambda_0^{-5}}{\bar{I}(T, \lambda_0)} + 1 \right)} \quad (4)$$

where h , c , and k are known constants (Planck's constant, the speed of light, and Boltzmann's constant, respectively).

III. METHODS

We evaluated the algorithms using three primary methods: 1) an intercomparison of retrieval performance with the simulation database as created with MODTRAN; 2) a comparison

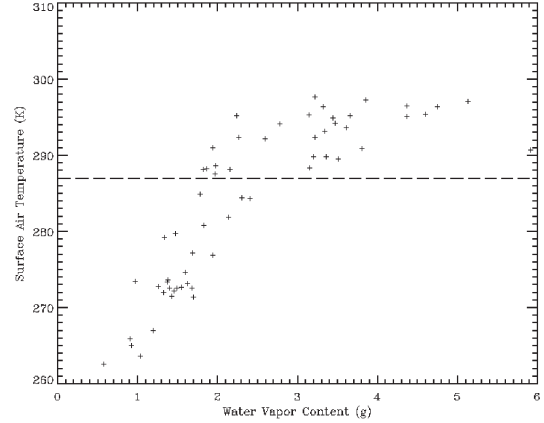


Fig. 3. SAT as a function of the total column water vapor of the 60 measured atmospheric profiles used in the simulation. The dashed line separates the profiles into two groups: (Above the line) warmer/moister atmospheres and (below the line) colder/drier atmospheres.

against the official MODIS LST product, where the tested algorithms were applied to the same TOA MODIS brightness temperature granules; and 3) a mathematical evaluation of algorithm sensitivity to errors in the prescribed surface emissivity. We did not evaluate the algorithms against the actual field measurements as we believe this could be misleading for at least four reasons: 1) LST algorithms are typically “tuned” against such field measurements before developing long-term global data sets, and to our knowledge, there is not a sufficient number of high-quality field data sets over diverse global-representative land covers to provide two independent statistically significant sample sets (one for “tuning” and one for performance testing); 2) most field measurements are at the point scale, and approaches to spatially scale-up point LST values to AVHRR/MODIS/VIIRS pixel sizes introduce uncertainties that are not easily quantified (particularly in the presence of structured surfaces with shadowing); 3) most field measurements are collected at nadir geometries and are not readily comparable to the off-nadir space-based samples (due to both LST and emissivity angular anisotropy); and 4) most field measurements are from broadband sensors, and the imprecise methods for determining and assigning emissivity values induce additional uncertainty when comparing the resulting LST against that from the relatively narrow-band space-based multispectral imagers.

A. Algorithm Intercomparison Within the Simulation Database

Following the approach used in developing the official MODIS algorithm [14], we stratified our simulated data according to the atmospheric regime: 1) “cold” atmospheres, where the SAT T_{air} is lower than 287 K (column water vapor ranged from about 0.5 to 2.4 g/cm²) and 2) “warm” atmospheres, where T_{air} is higher than 287 K (water vapor ranged from about 1.7 to 5.8 g/cm²). As shown in Fig. 3, this threshold roughly coincides with the point where the air temperature versus water vapor content relationship changes slope. This stratification acknowledges the capacity of warm atmospheres to hold more water vapor and the degradation of LST algorithm performance with increasing water vapor.

To better simulate real satellite data, we added Gaussian-distributed random noise to the modeled brightness temperatures. We set the standard deviation (STD) of the distribution to the sensor noise equivalent delta temperature values: $\sigma = 0.05$ K for MODIS and VIIRS and 0.12 K for AVHRR14 and AVHRR-16.

Because surface emissivity is an independent algorithm variable with relatively high uncertainty in practice, we also added Gaussian-distributed random noise to the prescribed emissivity values before conducting the regressions. The STD of the emissivity noise was set to 0.005, which is 2.5 times the digitization error of the MODIS emissivity product in bands 31 and 32.

Next, a regression analysis (emissivity values and TOA brightness temperatures versus prescribed LST) was performed to derive unique coefficients for each base algorithm and atmospheric condition (cold or warm). Following [14], the regressions were separately performed for the different subranges of the surface and air temperature differences, as well as for each subrange of the view zenith angle. We chose bins of $T_s - T_{\text{air}}$ as follows: -15 to -5 K, -5 to 2 K, 2 to 7 K, and 7 to 15 K. View zenith angle bins were defined in 10° angular increments from 0° to 70° . For the modified algorithms, we regressed the algorithms using data over the full range of view angles (0° to 70°).

B. Algorithm Evaluation Against Official MODIS Product

We also evaluated the algorithms against the official MODIS LST product (MOD11; Collection 4 reprocessing). Although the MODIS LST does not represent absolute ground “truth,” this product has been validated and shown to be accurate within 1 K [33] (see also <http://landval.gsfc.nasa.gov/ProductStatus.php?ProductID=MOD11>). In our previous work, we successfully used the MODIS LST product for the evaluation of the VIIRS LST algorithms [34]. Sixteen daytime MODIS Aqua swath scenes (2340 km \times 2330 km each) were selected for this purpose; eight from June 2004, representing warm atmospheric conditions, and eight from December 2004, representing the cold atmospheric conditions. At least 50% of the pixels in each scene were identified as “confident cloud free” from the MODIS cloud-screening procedure. All scenes were over North America.

Multiple supporting MODIS products were required for this analysis. TOA brightness temperatures were derived from the Level 1B radiance data (MOD02). The cloud screening was performed using the Level 2 cloud mask (MOD35). The LST (used as “truth”) and emissivity were obtained from the Level 3 MOD11, and the SAT was obtained from the Level 3 atmosphere profile product (MOD07). Swath geometric information was obtained from MOD03.

We computed the STD of the differences between the retrieved LSTs of each test algorithm and the official product (MOD11). The official product is based on [14], which is identified as algorithm 1 in the present paper (recall Table II). In MODIS operations, its coefficients are assigned from lookup tables indexed by atmospheric temperature (warm and cold), water vapor amount, and the temperature difference between

the surface (estimated) and the near-surface air. As needed, an interpolation procedure more precisely determines the coefficients for each pixel. This interpolation procedure and the coefficient stratification, as compared to our implementation, presumably lead to higher accuracy in the official MODIS LST product.

C. Theoretical Evaluation of Algorithm Formulations

In determining the algorithm coefficients in Section III-A, we applied Gaussian noise to the emissivity values prior to the regressions. As noted, we set the STD of the noise to 0.005. In reality, MODIS emissivity uncertainty may be much higher than that for a variety of reasons. For instance, a numerical inversion process alone may introduce a residual standard error in emissivity estimation of about 0.019 for the bands 31 and 32 [35]. The emissivity uncertainty will be even greater when estimated from land-cover mapping methods (e.g., [32]), because global land-cover maps are typically not updated often and their number of land-cover types is very limited.

Therefore, to estimate the sensitivity of each algorithm to emissivity errors, we derived the partial derivatives $\partial T/\partial \epsilon$ and $\partial T/\partial(\Delta \epsilon)$. The mathematical steps are provided in the Appendix. To determine the values of the resulting equations, we then prescribed reasonable values of temperature and emissivity, as will be shown in Section IV.

IV. RESULTS

We systematically compared the algorithms’ performance for the different satellite sensors, atmospheric conditions (warm and cold), land-air temperature differences, view angles, and sensitivity to the surface emissivity. Because the bias errors the regression analysis described in Section III were very small (less than 0.1 K), we characterize the algorithm performance here in terms of the LST precision, which in this paper was defined as the STD of the regressions. We made this decision for two reasons: 1) the precision statistic is not affected by the inevitable biases (offsets) in the radiation transfer model and 2) LST bias errors are typically resolved through on-orbit calibration of operational algorithms. Precision errors cannot be resolved in a similar manner, and therefore, we believe that precision serves as a more valuable and credible comparison metric for this paper. The results are presented in the following subsections.

A. Algorithm Similarity

For each of the 18 algorithms considered, we determined the STD of the regression that is fit for every combination of sensor, $T_s - T_{\text{air}}$ subrange, atmospheric regime, and view angle subrange. As an example, Fig. 4 shows the base algorithm results for MODIS Aqua under cold atmospheric conditions. The STD errors are presented as a function of the SAT difference (line patterns) and view zenith angle (x -axis). Three distinct groups of similar algorithm behavior are obvious in these results. For example, the results for algorithms 3 and

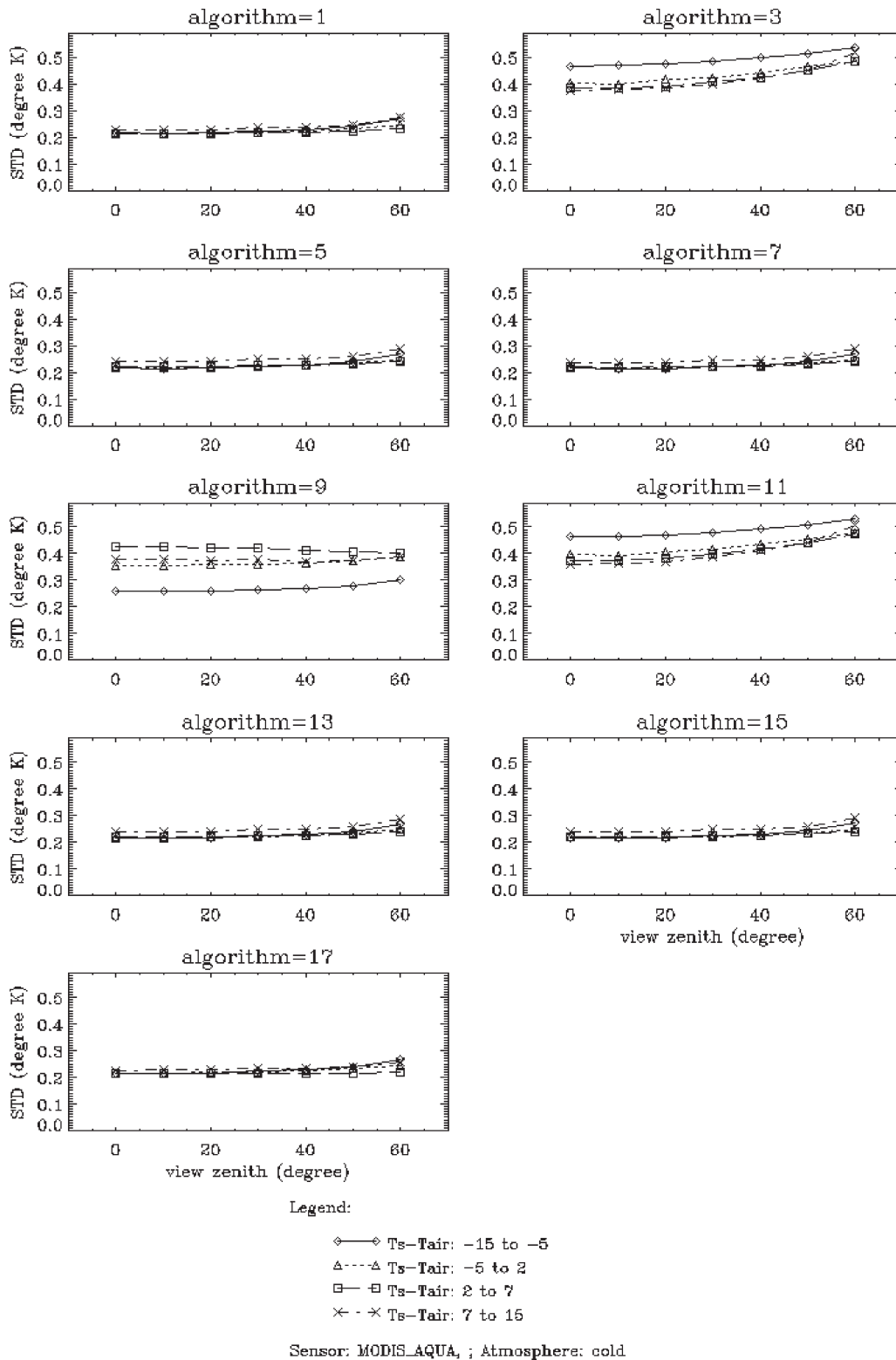


Fig. 4. STD errors of the regressions of the LST algorithms (listed in Table II) against the simulation data for the MODIS Aqua sensor under the cold atmospheric conditions.

11 are nearly identical in shape and magnitude. This led to our formation of algorithm groups (see Table III). This performance similarity among algorithm groups was apparent for all sensors and atmospheric conditions (warm and cold; not shown here).

Because of the performance similarity, we will provide results in some cases hereafter only for one algorithm representative of a group. Specifically, we will represent Group 1 with algorithm 13, Group 2 with algorithm 9, and Group 3 with algorithm 11. Other algorithms in a given group

TABLE III
ALGORITHM STRATIFIED BY PERFORMANCE SIMILARITY

Group Number	MEMBER ALGORITHMS
1	1, 5, 7, 13, 15, 17
2	9
3	3, 11

can be assumed to exhibit similar performance in both magnitude and trend.

B. Path-Length Correction

Regardless of algorithm or group, Fig. 4 reveals that the STD error generally increased as the view zenith angle increased. This effect was even stronger with warm atmospheres. This result is expected because SW algorithms are sensitive to water vapor in the view direction, and atmospheric path length (and hence, path water vapor content) approximately increases with $\sec(\theta)$.

As noted in Section I, we attempted to account for this view angle effect by introducing a path-length correction to the base (odd-numbered) algorithms; these modified algorithms were assigned with even numbers for clarity. To evaluate the effectiveness of the path-length correction term, we investigated the difference of the STD values between each base and associated modified algorithm. Recall that the base algorithms were uniquely tuned through independent regression for each 10° view zenith angle subrange, and the modified algorithms were regressed once simultaneously using all angles.

Fig. 5 provides examples of the view angle effect and path correction results. Specifically, we show three different STD errors: 1) LST_odd_all represents the base algorithms regressed with simulated data over all view angles (i.e., without using the 10° view zenith stratification); 2) LST_odd represents the base algorithms independently regressed with data from each successive 10° view zenith angle bin; and 3) LST_even represents the even-numbered algorithms (base algorithm with additional path-length correction term) regressed with data over all angles (as per the LST_odd_all case). As expected, the view angle effect is more obvious under the warm versus the cold atmospheric conditions. This is particularly true for algorithms 9 and 10 (representing Group 2). In the warm atmosphere cases, the angle effect is more significant at small view zenith angles. This is because when using one coefficient set for all view angles, retrieval accuracy at small angles is significantly worsened by the larger errors at large angles. Most importantly, Fig. 5 shows that the differences between the angularly stratified base algorithm (LST_odd) and modified algorithm (LST_even) were negligible; the two approaches are essentially equally effective. Given the greater simplicity of the single-coefficient set used with the even-numbered algorithms, we will only provide the results from the even-numbered algorithms in the following subsections.

C. Sensitivity to Sensor

To better understand the algorithm sensitivity to the sensor types, we evaluated the performance of each algorithm

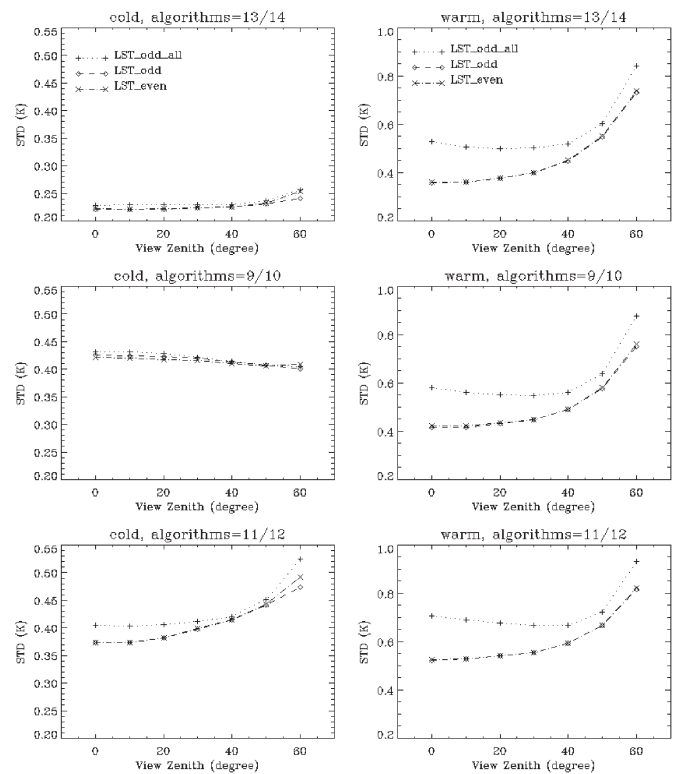


Fig. 5. STD errors of the different retrieval methods performed on the simulation data set where the $T_s - T_{\text{air}}$ difference is in the range of 2–7 K. In the plots, LST_odd_all represents the odd-numbered algorithms (base algorithms) without view angle stratification (i.e., one coefficient set for all the angles), LST_odd represents the odd-numbered algorithms with view zenith angle view angle stratification for the coefficient sets, and LST_even represents the even-numbered algorithms (base algorithm with additional path-length correction term). (Top, middle and bottom panels) Algorithms in groups 1, 2, and 3, respectively. (Left panels) Cold atmospheric conditions. (Right panels) Warm atmospheric conditions. The results are for the MODIS AQUA sensor. It is not clear which correction is superior after 50° . It is likely that both are degrading (at different rates) because most approximations of the radiative transfer equation (e.g., the SW approach) markedly degrade at high view zenith angles.

over the five sensors by comparing the mean precision error computed over all view angles and all $T_s - T_{\text{air}}$ values. The results are given in Table IV where the overall STD value is presented for the algorithm subgroups and for different sensors. For each algorithm, the performance did not significantly change across the different sensors, but the precision error over the warm atmosphere is about two to three times higher than that over the cold atmosphere. Furthermore, Group 1 outperformed Group 2, and both groups outperformed Group 3. These differences were most apparent for colder atmospheres.

Qualitatively, we found that the algorithms showed similar trends and behaviors across the different sensors throughout our paper. Therefore, for brevity, we generally show only the results for MODIS Aqua when discussing the results below.

D. Performance With Atmospheric Condition

As stated in [14], the stratification of algorithm coefficients by atmospheric condition improves retrieval performance. In practice, however, determination of SAT can be difficult.

TABLE IV
MEAN STDs [K] OF THE ALGORITHM REGRESSIONS FOR THE DIFFERENT SENSORS. TABLE VALUE EQUALS THE MEAN OF THE STD ERRORS OVER ALL $T_s - T_{air}$ CONDITIONS

Algorithm	MODIS Aqua	MODIS Terra	VIIRS	AVHRR-14	AVHRR-16
Cold Atmosphere					
Group 1					
2	0.23	0.23	0.24	0.26	0.29
6	0.24	0.24	0.24	0.26	0.29
8	0.24	0.24	0.24	0.26	0.29
14	0.24	0.24	0.24	0.26	0.29
16	0.24	0.24	0.24	0.26	0.29
18	0.23	0.23	0.24	0.26	0.28
Group 2					
10	0.36	0.36	0.35	0.37	0.39
Group 3					
4	0.45	0.45	0.39	0.41	0.42
12	0.44	0.44	0.38	0.40	0.41
Warm Atmosphere					
Group 1					
2	0.68	0.68	0.68	0.66	0.74
6	0.70	0.70	0.69	0.68	0.75
8	0.70	0.70	0.69	0.67	0.75
14	0.70	0.70	0.69	0.68	0.75
16	0.70	0.70	0.69	0.68	0.75
18	0.69	0.69	0.67	0.66	0.73
Group 2					
10	0.73	0.73	0.71	0.70	0.78
Group 3					
4	0.79	0.79	0.75	0.74	0.81
12	0.79	0.79	0.74	0.73	0.81

Without that knowledge, there is uncertainty as to which coefficient set (warm versus cold) to use with a given pixel. We therefore evaluated the LST errors that would be incurred by assuming the wrong atmospheric state, i.e., if algorithm coefficients for a warm atmosphere were applied to data collected over a cold atmosphere or vice versa.

The results differed by atmospheric regime and algorithm, but were relatively consistent across the sensors. Fig. 6 shows the results from the three representative algorithms for the MODIS Aqua sensor, in which the additional STD error is defined as the absolute STD difference between retrievals using the correct and incorrect coefficients.

Several trends are evident in the results. First, algorithm performance was sometimes highly sensitive to $T_s - T_{air}$. This is most evident for Group 3. For Groups 1 and 2, the additional errors were similar and relatively small for most $T_s - T_{air}$ cases, but were anomalously high with colder atmospheres (top panel in Fig. 6) when $-15 < T_s - T_{air} < -5$. The latter conditions can be common on clear nights in some regions.

Second, in most cases, the increased STD error is greater when the warm coefficients were used with a cold atmosphere (top panel) rather than vice versa (bottom panel). For instance, the extreme case for cold atmospheres is algorithm 14 (representing Group 1), where the additional error is up to 0.70 K. For warm atmospheres, the extreme case is algorithm 12 (representing Group 3), where the additional error is up to 0.90 K.

In general, the increase in errors with colder atmospheres is more significant than for warmer ones, considering that the initial errors are much smaller for the former. The increase in

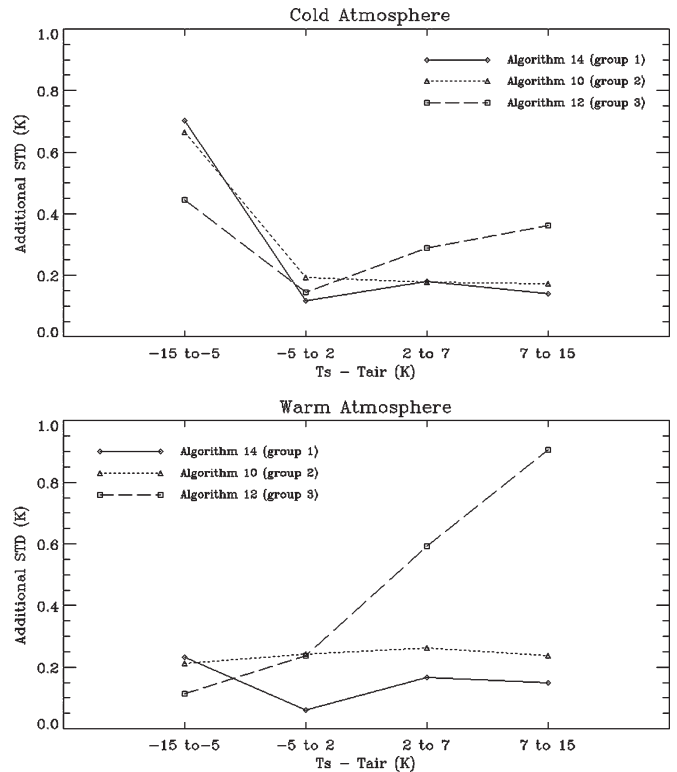


Fig. 6. (Top panel) Additional STD errors that occur if the coefficients derived for the warm atmospheric conditions are used with the cold atmospheric conditions (Bottom panel) Additional STD errors that occur if the coefficients for the cold atmospheric conditions are used with the warm atmospheric conditions. The results are for the MODIS AQUA sensor.

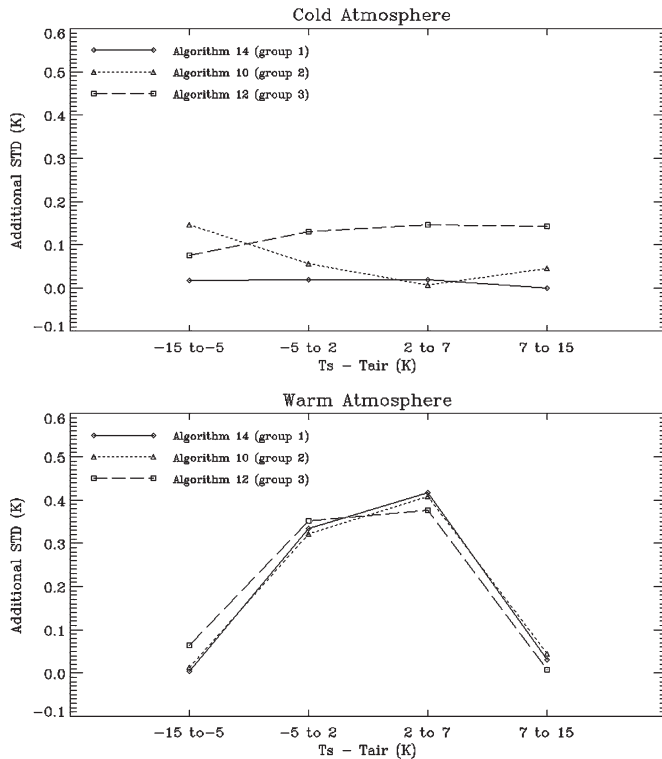


Fig. 7. Additional STD errors that occur if the algorithm coefficients are derived without stratification by the $T_s - T_{\text{air}}$ differences in the simulation database. The results are for the MODIS AQUA sensor.

errors over the warm atmospheres does not significantly vary across different $T_s - T_{\text{air}}$ values, except for Group 3 algorithms as previously noted.

E. Performance With $T_s - T_{\text{air}}$

Wan *et al.* [14] demonstrated that algorithm performance significantly improves if the algorithm is independently regressed for the different subranges of $T_s - T_{\text{air}}$ (the temperature difference between the land and surface air). To characterize this effect for different algorithms, we stratified the simulation data into four subranges of $T_s - T_{\text{air}}$ and independently determined the coefficients for each subrange. We compared the results with those obtained without such stratification.

In Fig. 7, we show the additional STD error incurred when there is no stratification of $T_s - T_{\text{air}}$. The three algorithm groups generally performed similarly. The additional error for cold atmospheres was relatively small for all conditions. This suggests that stratification can be ignored for the cold conditions. For warm atmospheres, however, the STD error increased by about 0.4 K when the air and surface temperatures are similar ($-5 < T_s - T_{\text{air}} < 7$ K). This agrees with the findings of [14] and confirms that LST precision error can be significantly reduced by stratifying coefficients by $T_s - T_{\text{air}}$ in warm atmospheric conditions. This finding was consistent for all the algorithms in this paper.

F. Performance Against Standard MODIS LST Product

As noted in Section III, the aforementioned analyses are only as good as the quality of the simulated satellite data. Con-

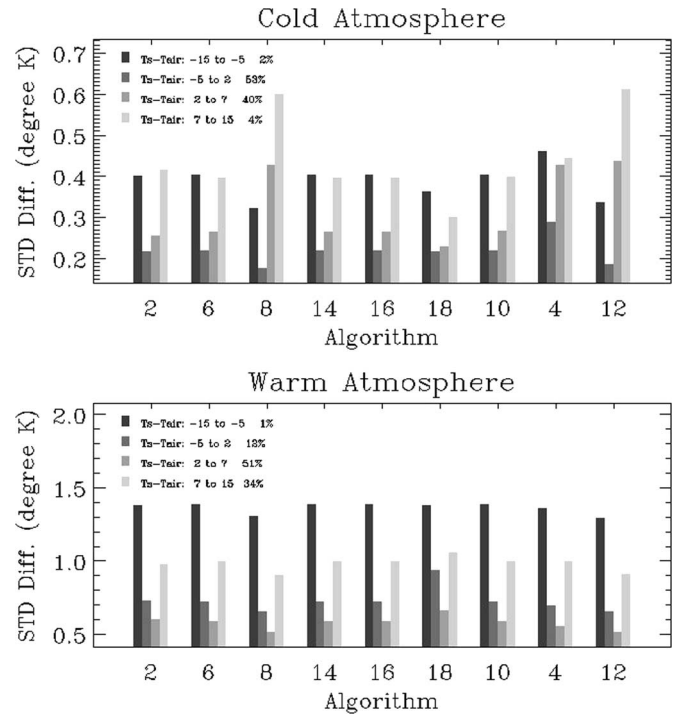


Fig. 8. STD of the performances of the modified algorithms against the official MODIS LST product (MOD11). Note that the algorithm order on the x -axis is arranged by group number and then by algorithm number. (Top panel) Eight winter scenes of the MODIS Aqua data were used to represent cold atmospheres. (Bottom panel) Eight summer scenes were used to represent warm atmospheres. All MODIS scenes were collected over North America in 2004, and each contains more than 50% cloud-free pixels.

sidering that all radiative transfer models require assumptions that limit their accuracy, we evaluated the heritage algorithms against the official MODIS LST product. Specifically, we used precision (i.e., STD) rather than accuracy as a measure in our evaluation process using the MODIS data, considering that: 1) MODIS LST data may be biased in certain regions and 2) the bias error (root-square difference between accuracy and precision) of the LST algorithm may be resolved through calibration in operational uses.

We determined the STD of the temperature difference between the LSTs derived using the modified algorithms and the MODIS LST products, as shown in Fig. 8. The STDs were stratified into four subranges of T_s and T_{air} difference. The top panel was derived from eight MODIS Aqua scenes in the winter of 2004, and the bottom panel was derived from eight MODIS Aqua scenes in the summer of 2004. The basic trends found in Sections IV-D and E were likewise found here. First, the retrieval errors against the official product significantly vary for the different subranges of $T_s - T_{\text{air}}$. The greater the temperature difference, the greater the error.

Note that in Fig. 8, we also give the fraction of pixels in each bin (see legend). For the majority of pixels, the LST is close to the SAT, particularly for cold atmospheres. Therefore, the error over the full range is close to the error derived for the smallest $|T_s - T_{\text{air}}|$ subranges. Table V gives the overall errors of the algorithms, where the errors are weighted by the mean of the errors for the different $T_s - T_{\text{air}}$ bins, and the weighting function is the fraction of pixels in each bin. For all

TABLE V
OVERALL STD [K] OF THE PERFORMANCES OF THE MODIFIED ALGORITHMS AGAINST THE OFFICIAL MODIS LST PRODUCT. THE ERRORS ARE THE WEIGHTED MEANS OF THE VALUES PLOTTED IN FIG. 8. THE WEIGHT IS THE FRACTION OF PIXELS IN EACH $T_s - T_{air}$ BIN

Algorithm	Winter	Summer
Group 1		
2	0.24	0.75
6	0.25	0.76
8	0.30	0.68
14	0.25	0.76
16	0.25	0.75
18	0.23	0.84
Group 2		
10	0.25	0.75
Group 3		
4	0.36	0.73
12	0.31	0.68

the algorithms, the errors against the MODIS LST are two to three times smaller in the winter than in the summer when the atmosphere is warmer and holds more water vapor.

We emphasize that the aforementioned results do not represent the STDs from “truth,” but are the STDs from the MODIS MOD11_L2 product, which has been validated to about 1 K uncertainty over several surface types (Wan, personal communication, 2005) [36]. Although the bias of the comparisons between the retrieved LST and the MODIS LST were not our primary focus for the aforementioned stated reasons, we found that they were in a range from -0.26 to -0.30 K for the winter case and from 0.70 to 0.89 K for the summer case, respectively, for the different algorithms.

G. Sensitivity to Emissivity Errors

We evaluated the algorithms’ sensitivity to emissivity errors using mathematical derivatives. Specifically, we derived the algorithm differential $[\delta(LST)]$ using the equations listed in Table II (see the Appendix) and plotted the temperature uncertainty against the emissivity uncertainty. The sample results (including the maximum and minimum sensitivities) are shown in Fig. 9. In calculating the results, we assumed that: 1) the mean emissivity and emissivity difference are 0.97 and 0.005 , respectively and 2) the brightness temperatures are 295 and 294 K for the $11\text{-}\mu\text{m}$ and $12\text{-}\mu\text{m}$ bands, respectively. It is clear that the LST errors increase approximately linearly, and that the magnitude of the errors can become very large (up to 6 K) for fairly small errors in emissivity.

V. DISCUSSION

Perhaps our most surprising finding was the tendency of multiple-heritage algorithms to perform very similarly over the various tests. This grouping behavior occurred across atmospheric conditions, but was most obvious with cold atmospheric conditions. The performance similarities led to our formulation of algorithm groups (Table III). We can now extend Table III to include qualitative performance information for cold atmospheres, as shown in Table VI.

A likely explanation for the performance similarity may be the algorithms’ similar functional dependence on emissivity. In Group 1, both the mean emissivity (ε) and the spectral emissivity difference ($\Delta\varepsilon$) are used in the algorithm formulas. In Group 2, emissivity in the $11\text{-}\mu\text{m}$ band is used instead of the mean emissivity, and the spectral emissivity difference is used together with the brightness temperature in the $12\text{-}\mu\text{m}$ band. In Group 3, only the mean emissivity is used. Our tests with simulated data suggest that the combined use of mean and difference emissivity terms leads to more accurate retrievals and stability over a wider range of conditions. It is therefore encouraging that Group 1 has the most members.

It is important to point out, however, that the overall precision of the algorithms that is given in Table VI is based on the assumption that accurate emissivity information is available (i.e., the emissivity uncertainty is less than 0.005). In practice, this requirement is hard to meet, and therefore, the LST precision may be worse. Indeed, our results (see Fig. 9) suggest that sensitivity to emissivity may be the most important factor in selecting an LST algorithm, at least until accurate and validated moderate resolution emissivity maps become available. It is obvious that algorithms 11/12 (Group 3) are much less sensitive to emissivity errors than those in Groups 1 and 2, because Group 3 algorithms do not use an emissivity difference ($\Delta\varepsilon$) term in their formulations. Note that because the uncertainty of the emissivity difference is the sum of the two spectral emissivity uncertainties, the derived temperature uncertainty is significantly enlarged. This is true for algorithms 13/14 (representing Group 1 algorithms) and 9/10 (Group 2), as shown in Fig. 9.

Although Table VI lists only the base algorithms, the modified algorithms show the same grouping behavior and thus belong in the same groups as their associated base algorithms. Indeed, performance differences between the base and associated modified algorithms were relatively small compared to the differences between groups. In a few cases, the modified algorithms outperformed the base algorithms (see Fig. 5).

In practice, the use of a modified algorithm, rather than regressing a base algorithm over multiple view angle subranges, is advantageous in that 1) it simplifies the regression analysis and lookup table structure that are used to determine and store the coefficients for operational algorithms and 2) it reduces the number of algorithm variants that must be validated with the sensor in orbit. We therefore suggest the modified algorithms are more economical for large-scale applications.

The implications of our study on CDRs are mixed. The consistency in algorithm results over different satellite sensors—particularly in the warm atmospheric cases—is promising (perhaps a prerequisite) for the development of a multidecadal LST CDR. It is particularly worth noting that the results for VIIRS and MODIS were so similar, despite the wide AVHRR-like bandpasses on VIIRS. This may suggest that bandwidth and band center specifications may be less important than the degree to which the spectral response function has a more Gaussian unimodal shape (recall Fig. 2). It is expected that the VIIRS bands will exhibit such shapes, despite the fact that AVHRR-16 did not.

The most obvious and consistent trend in our results was the superior algorithm performance in cold rather than warm

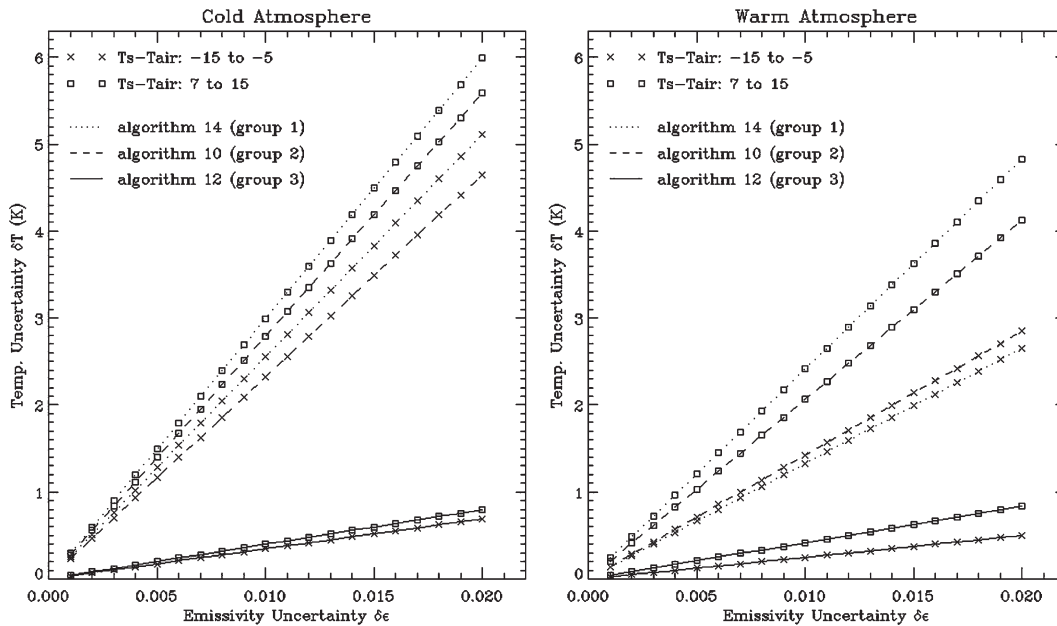


Fig. 9. Algorithm sensitivity to emissivity errors for the three algorithm groups from Table IV (represented by algorithms 14, 10, and 12). The results are for a mean emissivity of 0.97 and an emissivity difference of 0.005. The algorithm coefficients were derived from the MODIS Aqua simulation data over (left panel) the cold and (right panel) warm atmospheres. Only the cases of extreme T_s and T_{air} differences are plotted. For each algorithm, the results for the other $T_s - T_{air}$ bins fall between the cases shown. The results for all the other algorithms considered in this paper fall between those of algorithms 12 and 14.

TABLE VI
ALGORITHM PERFORMANCE OVER COLD ATMOSPHERES BY GROUP

Group	PRECISION ERROR	SENSITIVITY TO				MEMBER ALGORITHMS
	Overall	Emissivity Error	Sensor Type	View Zenith	$T_s - T_{air}$	
1	Low	Medium	Medium	Medium	Low	1, 5, 7, 13, 15, 17
2	Medium	High	Low	Low	Medium	9
3	Medium	Low	Low	Medium	Medium	3, 11

atmospheres. This was expected and relates to the relationship between air temperature and water-holding capacity (i.e., Clausius-Clapyron equation) and the imperfect atmospheric correction exhibited by the SW algorithms. This implies that LST CDR precision could be better in colder locations (e.g., high latitudes) and during midlatitude winters. The same factors (water vapor effects) explain the degradation in precision as view zenith angle increases (Fig. 4 and Fig. 5). To minimize this effect, a CDR algorithm might only use observations up to about $VZA = 50^\circ$. This approach may be feasible at high latitudes where multiple observations per day per satellite are collected. However, at lower latitudes, cloudiness and small swath overlap areas (or no overlap) from consecutive orbits usually preclude view angle filtering of daily products. Interestingly, however, all algorithms performed more consistently over warm atmospheres. Although one might conclude that algorithm choice is therefore less important in warm cases, the high-precision errors in those cases suggest that algorithm selection remains very important—even if the marginal improvement is small.

A more significant concern is the performance degradation for high values of T_s and T_{air} difference—particularly over warm atmospheres. This is particularly important at times of

day when the surface and air temperature differences are largest (e.g., just before sunrise or just after noon). Unfortunately, these times are often considered best for LST assessment because they can reveal the diurnal temperature range—a potential proxy for soil moisture [37]. Sampling at these times is also desirable because the time rate of change in LST tends to be lowest at these times such that edge-of-scan measurements on opposite sides of a swath are most comparable.

It may be possible to decrease sensitivity to $T_s - T_{air}$ through the greater stratification of coefficients during regression analysis, adapting the approach used with the MODIS operational algorithm for atmospheric temperature states. For example, a two-step LST retrieval could be applied, where the first retrieval is combined with air temperature information (e.g., from forecast models, sounder data or climatology [38]) to estimate $T_s - T_{air}$, and that value is used to determine the proper algorithm coefficient set for the final LST retrieval.

It is worth pointing out that we did not explicitly ensure seamless algorithm performance across the cold and warm threshold. That would indeed be an important concern if we were to actually apply an algorithm to satellite data for purposes of generating a data product. However, that criterion is not required for our purposes of intercomparing algorithm

performance across different sampling and environmental conditions.

VI. CONCLUSION

We conclude that: 1) a unified and coherent LST CDR developed with data from AVHRR, MODIS, and VIIRS is possible using a single algorithm uniquely tuned (i.e., unique coefficients) for each sensor; 2) an atmospheric path-length term can be added to heritage LST algorithms to significantly reduce their sensitivity to view zenith angle effects; 3) for practical purposes, just three heritage SW LST algorithms effectively exist because the published algorithms considered here can be assigned to one of the three groups defined by highly consistent performance characteristics; 4) precision errors significantly increase as $|T_s - T_{\text{air}}|$ increases, particularly in warm atmosphere cases; 5) algorithms that depend on both the band emissivities (ε_{11} and ε_{12}) and the spectral emissivity difference ($\Delta\varepsilon$) tend to be more accurate than other algorithms when emissivity values are well known *a priori*, and 6) algorithms that do not depend on the spectral emissivity difference are less sensitive to emissivity errors and, thus, may be more robust when land emissivity is not well known.

We conclude that a Group 1 algorithm would be best for CDR development in areas where surface emissivity is well known and varies little in time and space, such as over large semi-homogeneous land covers like deserts and dense evergreen forests. In more heterogeneous conditions, we conclude that algorithms 3/4 (based on Prata and Platt [16] and Caselles *et al.* [17]) or 11/12 (based on Ulivieri *et al.* [21]) are preferable, given their lower sensitivity to emissivity errors and acceptable precision performance under different conditions.

APPENDIX

The total LST uncertainty δT_s due to the emissivity uncertainty can be explained in

$$\delta T_s = \sqrt{\delta T_1^2 + \delta T_2^2}$$

where ΔT_1 and δT_2 represent the uncertainty contributed from the uncertainties of emissivity (ε) uncertainty and emissivity difference ($\Delta\varepsilon$), respectively. Take algorithm 14 as an example. These two components are

$$\delta T_1 = \left(A_3 - \frac{A_4}{\varepsilon^2} \right) \delta\varepsilon$$

and

$$\delta T_2 = \frac{A_4}{\varepsilon} \delta(\Delta\varepsilon).$$

Therefore, the total LST uncertainty for algorithm 14 is

$$\delta T_s = \sqrt{\left[\left(A_3 - \frac{A_4}{\varepsilon^2} \right) \delta\varepsilon \right]^2 + \left[\frac{A_4}{\varepsilon} \delta(\Delta\varepsilon) \right]^2}.$$

Similarly, the total LST uncertainty for algorithm 12 is

$$\delta T_s = \sqrt{[A_3(T_{11} - T_{12})\delta\varepsilon_{11}]^2 + [A_4 T_{12} \delta(\Delta\varepsilon)]^2}.$$

Coefficients A_3 and A_4 were calculated in the regression analysis using the simulation data. Considering that $\varepsilon = (\varepsilon_{11} + \varepsilon_{12})/2$ and $\Delta\varepsilon = (\varepsilon_{11} - \varepsilon_{12})$, and assuming the emissivity uncertainties in each band are the same, i.e., $\delta\varepsilon = \delta\varepsilon_{11} = \delta\varepsilon_{12}$, the uncertainty of the emissivity difference is $\delta(\Delta\varepsilon) = |\delta\varepsilon_{11}| + |\delta\varepsilon_{12}| = 2\delta\varepsilon$.

ACKNOWLEDGMENT

The authors would like to thank B. Hauss and A. Sei of Northrop Grumman Space Technology for providing helpful advice on applying emissivity noise and Ron Vogel for assisting with various computations. The authors would also like to thank the Goddard Earth Sciences Distributed Active Archive Center (DAAC) and the Land Processes DAAC, Sioux Fall, South Dakota, for the Moderate Resolution Imaging Spectroradiometer (MODIS) products used here and the Department of Geography, Boston University where they acquired the MODIS surface type data online.

The manuscript contents are solely the opinions of the author(s) and do not constitute a statement of policy, decision, or position on behalf of NOAA or the U.S. Government.

REFERENCES

- [1] J. M. Norman and F. Becker, "Terminology in thermal infrared remote sensing of natural surfaces," *Agric. For. Meteorol.*, vol. 77, no. 3, pp. 153–166, Dec. 1995.
- [2] W. P. Kustas and J. M. Norman, "Use of remote sensing for evapotranspiration monitoring over land surfaces," *Hydrol. Sci. J.*, vol. 41, no. 4, pp. 495–515, Aug. 1996.
- [3] M. Jin, "Analysis of land skin temperature using AVHRR observations," *Bull. Amer. Meteorol. Soc.*, vol. 85, no. 4, pp. 587–600, Apr. 2004.
- [4] National Research Council, *Climate Data Records From Environmental Satellites*, 2004, Washington, DC: Nat. Academies Press.
- [5] National Research Council, *Review of NOAA's Plan for the Scientific Stewardship Program*. Washington, DC: Nat. Academies Press, 2005.
- [6] R. S. Stolarski and S. M. Frith, "Search for evidence of trend slow-down in the long-term TOMS/SBUV total ozone data record: The importance of instrument drift uncertainty," *Atmos. Chem. Phys.*, vol. 6, no. 12, pp. 4057–4065, 2006.
- [7] K. S. Casey and R. W. Reynolds, "Development and application of the SST climate data record from space," in *Proc. Ocean Sci. Meeting*, Honolulu, HI, Feb. 2006.
- [8] L. M. McMillin and D. S. Crosby, "Theory and validation of the multiple window sea surface temperature technique," *J. Geophys. Res.*, vol. 89, no. C7, pp. 3655–3661, 1984.
- [9] H. Ouaidrari, S. N. Goward, K. P. Czajkowski, J. A. Sobrino, and E. Vermote, "Land surface temperature estimation from AVHRR thermal infrared measurements: An assessment for the AVHRR Land Pathfinder II data set," *Remote Sens. Environ.*, vol. 81, no. 1, pp. 114–128, Jul. 2002.
- [10] D. P. Vazquez, F. J. O. Reyes, and L. A. Arboledas, "A comparative study of algorithms for estimation of land surface temperature from AVHRR," *Remote Sens. Environ.*, vol. 62, pp. 215–222, 1997.
- [11] Y. H. Kerr, *Land Surface Temperature Retrieval Techniques and Applications (Case of the AVHRR)*, 2000. [Online]. Available: http://www.cetp.ipsl.fr/1activ/21mineu/iot/publi_pdf/IRT-Book-YHK.pdf
- [12] A. C. Pinheiro, J. L. Privette, R. Mahoney, and C. J. Tucker, "Directional effects in a daily AVHRR land surface temperature dataset over Africa," *IEEE Trans. Geosci. Remote Sens.*, vol. 42, no. 9, pp. 1941–1954, Sep. 2004.
- [13] Z. Wan and Z.-L. Li, "A physics-based algorithm for retrieving land surface emissivity and temperature from EOS/MODIS data," *IEEE Trans. Geosci. Remote Sens.*, vol. 35, no. 4, pp. 980–996, Jul. 1997.

- [14] Z. J. Wan and J. Dozier, "A generalized split-window algorithm for retrieving land surface temperature from space," *IEEE Trans. Geosci. Remote Sens.*, vol. 34, no. 4, pp. 892–905, Jul. 1996.
- [15] F. Becker and Z.-L. Li, "Toward a local split window method over land surface," *Int. J. Remote Sens.*, vol. 11, no. 3, pp. 369–393, 1990.
- [16] A. J. Prata and C. M. R. Platt, "Land surface temperature measurements from the AVHRR," in *Proc. 5th AVHRR Data Users Conf.*, Tromsø, Norway, Jun. 25–28, 1991, pp. 438–443. EUM P09.
- [17] V. Caselles, C. Coll, and E. Valor, "Land surface temperature determination in the whole Hapex Sahell area from AVHRR data," *Int. J. Remote Sens.*, vol. 18, no. 5, pp. 1009–1027, 1997.
- [18] C. Olivieri, M. M. Castronovo, R. Francioni, and A. Cardillo, "A SW algorithm for estimating land surface temperature from satellites," *Adv. Space Res.*, vol. 14, no. 3, pp. 59–65, 1992.
- [19] A. Vidal, "Atmospheric and emissivity correction of land surface temperature measured from satellite using ground measurements or satellite data," *Int. J. Remote Sens.*, vol. 12, no. 12, pp. 2449–2460, 1991.
- [20] J. C. Price, "Land surface temperature measurements from the split window channels of the NOAA 7 Advanced Very High Resolution Radiometer," *J. Geophys. Res.*, vol. 89, no. D5, pp. 7231–7237, 1984.
- [21] C. Olivieri and G. Cannizzaro, "Land surface temperature retrievals from satellite measurements," *Acta Astronaut.*, vol. 12, no. 12, pp. 985–997, 1985.
- [22] J. A. Sobrino, Z. L. Li, M. P. Stoll, and F. Becker, "Improvements in the split-window technique for land surface temperature determination," *IEEE Trans. Geosci. Remote Sens.*, vol. 32, no. 2, pp. 243–253, Mar. 1994.
- [23] C. Coll, E. Valor, T. Schmugge, and V. Caselles, "A procedure for estimating the land surface emissivity difference in the AVHRR channels 4 and 5," *Remote Sensing Application to the Valencian Area, Spain*, 1997.
- [24] J. A. Sobrino, Z. L. Li, M. P. Stoll, and F. Becker, "Determination of the surface temperature from ATSR data," in *Proc. 25th Int. Symp. Remote Sens. Environ.*, Graz, Austria, Apr. 4–8, 1993, pp. II-19–II-109.
- [25] E. P. McClain, W. G. Pichel, and C. C. Walton, "Comparative performance of AVHRR-based multichannel sea surface temperatures," *J. Geophys. Res.*, vol. 90, no. C14, pp. 11 587–11 601, 1985.
- [26] C. Walton, W. Pichel, J. Sapper, and D. May, "The development and operational application of nonlinear algorithms for the measurement of sea surface temperatures with the NOAA polar-orbiting environmental satellites," *J. Geophys. Res.*, vol. 103, no. C12, pp. 27 999–28 012, 1998.
- [27] J. Ip and B. Hauss, *Development and Testing of the VIIRS Land Surface Temperature Using Global MODIS Proxy Data and Global Synthetic Data*, 2007. [Online]. Available: http://npoesslib.ipnoaa.gov/IPOarchive/ED/Outreach_Materials/public_presentations/AMS/2007/Posters/S2-P28-120356-Final-Ip-Hauss.pdf
- [28] D. Sun and R. T. Pinker, "Estimation of land surface temperature from a Geostationary Operational Environmental Satellite (GOES-8)," *J. Geophys. Res.*, vol. 108, no. D11, p. 4326, 2003.
- [29] D. Sun and R. T. Pinker, "Implementation of GOES-based land surface temperature diurnal cycle to AVHRR," *Int. J. Remote Sens.*, vol. 26, no. 18, pp. 3975–3984, Sep. 2005.
- [30] Y. Yu, D. Tarpley, J. P. Privette, M. K. Rama Varma Raja, and H. Xu, "Developing split window algorithm for land surface temperature measurement from GOES-R ABI sensor: Part 1, Retrieval analysis," in *Proc. GOES-R Algorithm Working Group Annu. Meeting*, 2007.
- [31] A. Berk, G. P. Anderson, P. K. Acharya, J. H. Chetwynd, M. L. Hoke, L. S. Bernstein, E. P. Shettle, M. W. Matthew, and S. M. Alder-Golden, *MODTRAN4 Version 2 Users's Manual*. Hanscom AFB, MA: Space Vehicles Directorate, Apr. 2000.
- [32] W. C. Snyder, Z. Wan, and Y. Z. Feng, "Classification-based emissivity for land surface temperature measurement from space," *Int. J. Remote Sens.*, vol. 19, no. 14, pp. 2753–2774, Sep. 1998.
- [33] Z. Wan, Y. Zhang, Q. Zhang, and Z.-L. Li, "Validation of the land-surface temperature products retrieved from Terra Moderate Resolution Imaging Spectroradiometer data," *Remote Sens. Environ.*, vol. 83, no. 1, pp. 163–181, Nov. 2002.
- [34] Y. Yu, J. L. Privette, and A. C. Pinheiro, "Analysis of the NPOESS VIIRS land surface temperature algorithm using MODIS data," *IEEE Trans. Geosci. Remote Sens.*, vol. 43, no. 10, pp. 2340–2350, Oct. 2005.
- [35] S. Liang, "Inversion of land surface temperature and emissivity simultaneously from multispectral thermal infrared imagery," in *Proc. IGARSS*, 2000, pp. 3133–3135.
- [36] C. Coll, V. Caselles, J. M. Galve, E. Valor, R. Niclos, J. M. Sanchez, and R. Rivas, "Ground measurements for the validation of land surface temperatures derived from AATSR and MODIS data," *Remote Sens. Environ.*, vol. 97, no. 3, pp. 288–300, Aug. 2005.
- [37] A. C. Pinheiro, C. J. Tucker, D. Entekhabi, J. L. Privette, and J. A. Berry, "Assessing the relationship between surface temperature and soil moisture in southern Africa," in *Remote Sensing and Hydrology*, M. Owe, K. Brubaker *et al.*, Eds. Wallingford, U.K.: IAHS Press, 2001, pp. 296–301.
- [38] A. C. T. Pinheiro, J. Desclotres, J. L. Privette, J. Susskind, L. Iredell, and J. Schmaltz, "Near-real time retrievals of land surface temperature within the MODIS rapid response system," *Remote Sens. Environ.*, vol. 106, no. 3, pp. 326–336, Feb. 2007.



Yunyue Yu received the B.A. degree in physics from the Ocean University of Qingdao, Qingdao, China, in 1982, the diploma in physics from Peking University, Beijing, China, in 1986, and the Ph.D. degree in aerospace engineering sciences from the University of Colorado, Boulder, in 1996.

Before studying at the University of Colorado, he was an Associate Professor at the Ocean University of Qingdao where he worked on satellite ocean surface remote sensing. In 1997, he joined the Earth Observation System Satellites Program and worked

with the National Aeronautics and Space Administration Goddard Space Flight Center, Greenbelt, MD. He is currently a Physical Scientist with the National Oceanic and Atmospheric Administration, National Environmental Satellite, Data, and Information Service Center for Satellite Applications and Research, Camp Springs, MD. He is also land team chair of the Algorithms Working Group of the Geostationary Operational Environmental Satellite Series R Satellite Mission, and a Member of the National Polar-Orbiting Operational Environmental Satellite System Visible/Infrared Imager Radiometer Suite Operational Algorithm Team. Since 1986, he has accomplished a variety of projects in ocean and land surface remote sensing and applications.



Jeffrey L. Privette (M'96) received the B.S. degree from the University of Michigan, Ann Arbor, and The College of Wooster, Wooster, OH, and the M.S. and Ph.D. degrees in aerospace engineering sciences from the University of Colorado, Boulder, in 1994.

From 1996 to 2006, he worked at the National Aeronautics and Space Administration Goddard Space Flight Center, Greenbelt, MD, where he helped coordinate the Southern African Regional Science Initiative (SAFARI) 2000, the Moderate Resolution Imaging Spectroradiometer (MODIS)

Land Validation Program, the Committee on Earth Observation Satellites Working Group for Calibration and Validation Land Subgroup, and the National Polar-Orbiting Operational Environmental Satellite System (NPOESS) Preparatory Project (as a Deputy Project Scientist). In 2006, he joined the National Oceanic and Atmospheric Administration (NOAA) National Climatic Data Center, Asheville, NC, where he serves as a Land Lead of the NPOESS Visible/Infrared Imager Radiometer Suite (VIIRS) Operational Algorithm Team and a Project Scientist for NOAA's Scientific Data Stewardship Project. His research has mainly focused on the retrieval and validation of land biophysical parameters from wide field-of-view imagers (e.g., AVHRR, MODIS, VIIRS), with an emphasis on directional effects.



Ana C. Pinheiro received the B.S. degree in environmental engineering from the New University of Lisbon, Lisbon, Portugal, in 1995, the M.Eng. degree in civil and environmental engineering from the Massachusetts Institute of Technology, Cambridge, in 1998, and the Ph.D. degree in environmental engineering from the New University of Lisbon, in 2003. She conducted her doctoral research as a Visiting Scientist in the Biospheric Sciences Branch, National Aeronautics and Space Administration (NASA) Goddard Space Flight

Center (GSFC), Greenbelt, MD.

In November 2003, she joined the NASA GSFC Hydrological Sciences Branch as a National Research Council Postdoctoral Fellow and was a NASA Postdoctoral Program Fellow in the same branch from January 2006 to January 2007. In February 2007, she joined the National Oceanic and Atmospheric Administration National Climatic Data Center, Asheville, NC, as an STG Inc. Contractor.